

Correlations between flaw tolerance and reliability in zirconia

M. J. READEY, C. L. McCALLEN, P. D. McNAMARA

Department of Materials Science and Engineering, Carnegie Mellon University, Pittsburgh, PA 15213, USA

B. R. LAWN

Materials Science and Engineering Laboratory, National Institute of Standards and Technology, Gaithersburg, MD 20899, USA

Interrelations between flaw tolerance and reliability in Y-TZP, Ce-TZP and Mg-PSZ ceramics are investigated. Indentation–strength tests indicate an enhanced flaw tolerance with increasing *R*-curve behaviour from tetragonal → martensite transformation. The Weibull modulus of unindented specimens increases with the enhanced tolerance. However, even the most tolerant zirconias show persistent scatter in strength, implying that variability in material microstructure may be as important a factor in reliability evaluation in these materials as variability in flaw size.

1. Introduction

It is now well established that many engineering ceramics demonstrate pronounced crack-resistance (*R*-curve) behaviour, where fracture toughness increases with crack extension. One class of ceramics that shows particularly strong *R*-curves is zirconia, from transformation toughening [1–3]. A consequence of *R*-curve behaviour is “flaw tolerance”, meaning that the strength becomes less sensitive to initial flaw size relative to conventional ceramics which obey the Griffith failure criterion [4–6]. Recently, it has been suggested that flaw-tolerant ceramics may also exhibit a reduced variability in strength, with a consequent improved reliability [7–9]. While flaw tolerance has been extensively studied in alumina ceramics [4, 6, 10], the same is not true of zirconia ceramics. Moreover, definitive evidence for improved reliability due to flaw tolerance is not generally available.

The purpose of this preliminary study was to establish a correlation between flaw tolerance and reliability in Y-TZP, Ce-TZP and Mg-PSZ ceramics subjected to various heat treatments. Previous studies of similar materials have reported pronounced *R*-curve behaviour in Mg-PSZ and Ce-TZP ceramics [5, 11, 12], but little or none in Y-TZP ceramics [13]. First, we determined the flaw tolerance characteristics of our materials using indentation flaws [4, 6, 10]. Then we evaluated the strength variability of unindented specimens using conventional Weibull statistics. Conclusions were drawn concerning the competitive roles of flaw size and microstructural variability on the Weibull modulus.

2. Experimental procedure

2.1. Material processing

Y-TZP (3 mol %), Ce-TZP (12 mol%) and Mg-PSZ

(9 mol %) were chosen for study because of their well-documented toughness properties [11–17] and microstructural characteristics [17]. The toughening arises from transformation of constrained tetragonal (*t*) phase to monoclinic (*m*) phase. In TZP the *t*-phase pre-exists as complete grains, in PSZ as precipitates within a cubic matrix. Our general aim was to produce zirconias with different microstructures, and hence different flaw tolerances. More specifically, the aim was to vary the *R*-curves of our selected materials without altering the fundamental nature of the flaw populations, so that we might observe the influence of flaw tolerance on reliability in a well-controlled material system.

Specimens approximately 25 mm diameter by 4 mm thick were prepared by pressing powders to 70 MPa in a hardened steel die. The green compacts were then cold-isostatically pressed to 250 MPa, and heat treated for various times and temperatures. All materials were embedded in powder of the same composition to minimize volatilization, and sintered at specified temperatures and times in air using heating and cooling rates of 5 °C min⁻¹. The Mg-PSZ materials were subjected to additional post-sintering ageing heat treatments [14], after cooling directly from the sintering temperature at 10 °C min⁻¹. Heat-treatment details are included in Table I.

2.2. Microstructure analysis

Densities of the sintered ceramics were determined using Archimedes' method. Grain sizes were determined from scanning electron micrographs of polished and thermally etched surfaces using an image analysis system. Precipitate sizes in Mg-PSZ were measured on fracture surfaces after chemically etching in concentrated HF acid to remove the cubic matrix.

TABLE I Sintering/heat-treatment schedules for zirconia ceramics. (Mg-PSZ ageing carried out after quenching specimens from the sintering temperature)

Zirconia	Sintering temp. (°C)	Sintering time (min)	Ageing temp. (°C)	Ageing time (min)
Y-TZP ^a	1450	120	–	–
	1575	120	–	–
Ce-TZP ^b	1450	120	–	–
	1450	3000	–	–
Mg-PSZ ^c	1700	120	1400	0
	1700	120	1400	40
	1700	120	1400	60

^a SY-Ultra, Z-Tech Corporation, Bow, NH, USA.

^b TZ-12CE, Tosoh Ceramics, Tosoh Corporation, Tokyo.

^c TZ-9MG, Tosoh Ceramics, Tosoh Corporation, Tokyo.

X-ray diffraction (XRD) phase analysis was conducted on both as-polished surfaces and subsequent fracture surfaces. Integrated intensities of *m* and *t* {111} peaks were measured using a non-linear curve-fitting program. The *m*-phase fractions were evaluated using the method of Porter and Heuer [18]. The *t*-phase fractions that transformed during fracture were then determined as differences in *m*-phase fraction in the polished and fracture surfaces.

2.3. Flaw tolerance and reliability

The flaw tolerance of the zirconia ceramics was assessed using the indentation–strength test [4, 6, 10]. The discs were ground to a thickness of 2 mm and the prospective test surfaces diamond-polished to a finish of 1 μm. A Vickers microhardness indentation was placed at the centre of each test surface, at loads between 3 and 300 N. A small drop of oil was then placed on the indentation site to minimize environmentally assisted slow crack growth. The specimens were then rapidly loaded ($\approx 250 \text{ MPa s}^{-1}$) to failure in biaxial flexure using a flat-on-3-ball technique, with the indented surfaces on the tensile side. Strengths were determined from the equations of linear elasticity for thin plates. (We acknowledge these materials can show a marked non-linearity in their stress–strain responses, resulting in a shift of the neutral axis during loading. Thus our calculations will overestimate the actual strength [5].) The specimens were subsequently inspected to determine which failures originated from the indentation. Those which did not were excluded from the data set.

Strength variability for unindented specimens was quantified using conventional Weibull statistics. A minimum sample of 50 specimens of each batch of material was prepared by grinding and polishing, as discussed earlier. The specimens were broken in biaxial flexure without indentation, with the polished surfaces on the tensile side. The ensuing strength data were then analysed using a two-parameter Weibull function [19, 20].

3. Results

3.1. Density and grain size

All the materials had a density of $> 98\%$ theoretical in their as-sintered state. The microstructures of the Y-

TABLE II Physical properties of zirconia ceramics

Zirconia	Ageing treatment (°C min ⁻¹)	Density (Mg m ⁻³)	Grain size (μm)	Precipitate size (nm)
Y-TZP	1450/120	6.03	0.31	–
	1575/120	6.03	0.86	–
Ce-TZP	1450/120	6.17	0.56	–
	1450/3000	6.18	2.1	–
Mg-PSZ	1400/0	5.68	40	160
	1400/40	5.66	40	280
	1400/60	5.59	40	380

TZP and Ce-TZP ceramics were relatively uniform and equiaxed. The mean grain size of these two materials increased with heat treatment (final size $\approx 2.2 \mu\text{m}$). For the Mg-PSZ the microstructures were less regular, and coarser (grain size $\approx 40 \mu\text{m}$). The latter grain size was independent of post-sintering ageing time. Details are included in Table II.

3.2. Phase microstructure

XRD of as-polished surfaces revealed no *m*-phase in the as-sintered Y-TZP and Ce-TZP ceramics, suggesting that the grain sizes are well below those necessary for spontaneous transformation to the *m*-phase during cooling [21]. On the other hand, as seen in Fig. 1, significant transformation occurred during fracture, especially at the coarser grain sizes. The degree of transformation was substantially higher in Ce-TZP than in Y-TZP, consistent with a much higher steady-state toughness [17].

XRD of as-polished surfaces of Mg-PSZ again revealed no *m*-phase prior to ageing. However, some *m*-phase was observed after post-sintering ageing, indicating that a fraction of the precipitates must have coarsened beyond the critical size. SEM inspection of acid-etched surfaces indeed revealed ever-coarsening lenticular precipitate structures in these materials [18], over a particle length range 160–380 nm (Table II). The amount of transformation of the residual *t*-phase precipitates during subsequent fracture varied with ageing time, with a peak at $\approx 40 \text{ min}$, as seen in Fig. 1; accordingly, we refer to the three Mg-PSZ materials represented in Fig. 1 as under-aged, peak-aged, and over-aged.

3.3. Indentation flaws

Examinations of the indentation sites on polished zirconia surfaces revealed considerable variability. In the Y-TZP materials the indentations showed the well-known radial crack pattern. However, only at the higher loads were the patterns “well developed”, i.e. symmetrical with arms extending a distance of more than one impression half-diagonal from each corner. At the lower loads the patterns were more asymmetrical, with one or more ill-formed radial cracks less than one-tenth of an impression half-diagonal. Observations in Nomarski illumination showed evidence for significant contact-induced transformation zones surrounding the hardness impressions. These zones exert

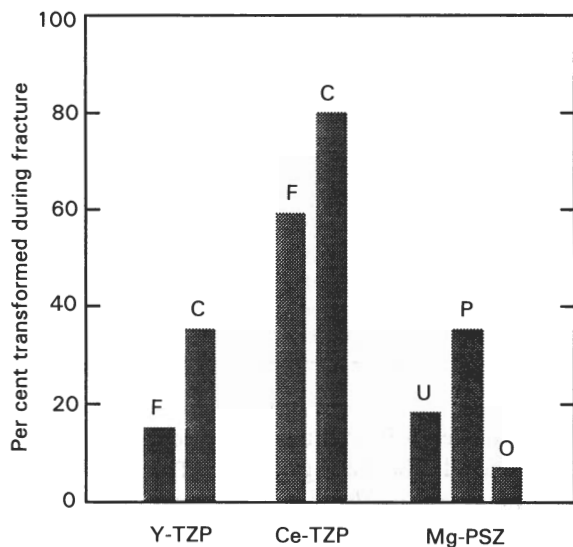


Figure 1 Percentage of t-phase transformed to m-phase during fracture of zirconia ceramics, as determined by comparative measurements on polished and fracture surfaces. For Y-TZP and Ce-TZP the fraction of transforming t-phase grains increases with change from finer (F) to coarser (C) grain scale. For Mg-PSZ the fraction increases with ageing from its initial value in the as-sintered state (under-aged, U) to a maximum (peak-aged, P) and then decreases (over-aged, O).

considerable compressive hoop stresses in the extra-hardness region, thereby “trapping” the incipient radial cracks in a subthreshold propagation state [22].

In the Ce-TZP and Mg-PSZ materials, the indentation fracture patterns were always ill formed, with little or no sign of radial extension beyond the hardness impression, except occasionally in the over-aged Mg-PSZ at the highest loads. These materials showed pronounced transformation zones outside the impression.

3.4. Flaw tolerance and Weibull modulus

3.4.1. Y-TZP

Indentation-strength data for the as-indentured Y-TZP ceramics are plotted in Fig. 2. The two materials show a parallel dependence on indentation load, close to the classical $-1/3$ slope (dashed line, logarithmic coordinates) characteristic of materials with single-valued toughnesses [4, 6]. Slight deviations toward a lower slope are observed at low loads; ultimately, the strength cuts off abruptly, corresponding to failures from competing processing flaws (boxes at left). The data for the coarser grained material lie just below their finer grained counterparts, indicating a slightly reduced toughness. We note that the indentation data show considerable scatter, reflecting some kind of intrinsic variability in the indentation flaw K -field in these materials.

Weibull plots for unindentured Y-TZP are shown in Fig. 3. The strength distributions for the two grain sizes are comparable, with relatively low Weibull moduli $m = 7.4$ (coarse) and $m = 9.0$ (fine).

3.4.2. Ce-TZP

Comparative indentation-strength data are plotted for Ce-TZP ceramics in Fig. 4. As with the Y-TZP, the

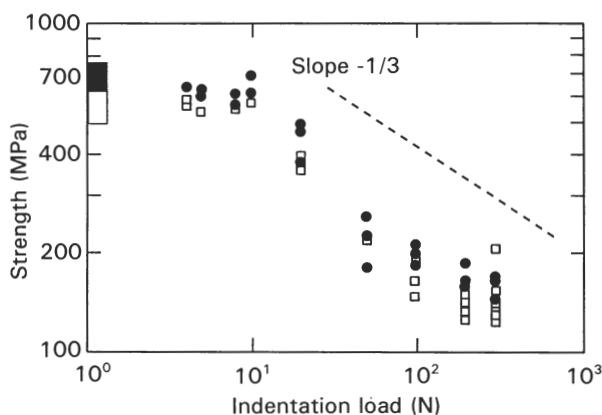


Figure 2 Strength as a function of indentation load for Y-TZP ceramics. Materials show strong sensitivity to load, and only slight dependence on grain size (cf. classical strength versus load $^{-1/3}$ dependence, ---). (●) Fine grain, (□) coarse grain.

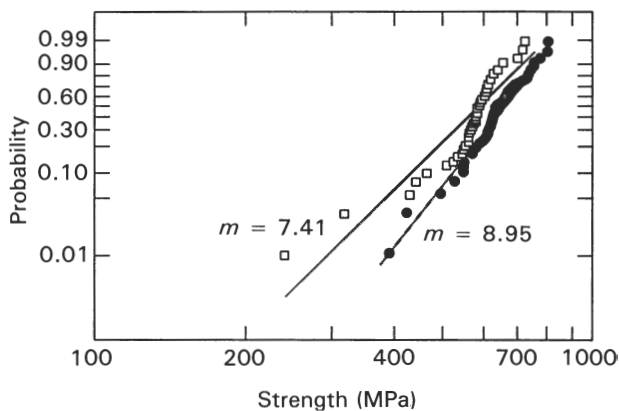


Figure 3 Weibull plots for Y-TZP ceramics. Note comparable Weibull moduli. (●) Fine grain, (□) coarse grain.

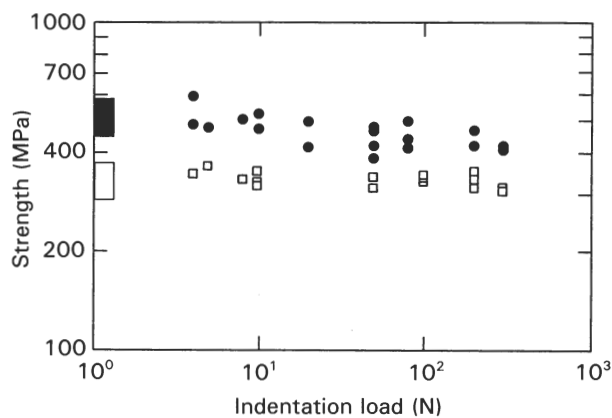


Figure 4 Strength as a function of indentation load for Ce-TZP ceramics. Materials show strong flaw tolerance (cf. Fig. 2). Coarser material shows lower strength but greater flaw tolerance. (●) Fine grain, (□) coarse grain.

finer grain-sized material is stronger. Now, however, the strengths are nearly invariant with indentation load, diminishing by $< 5\%$ over the load range for the coarser material and $< 15\%$ for the finer. The strength data no longer cut off abruptly at the levels for failure from natural flaws (boxes at left), but approach these levels asymptotically. These zirconias are therefore, relatively flaw tolerant, indicative of a ma-

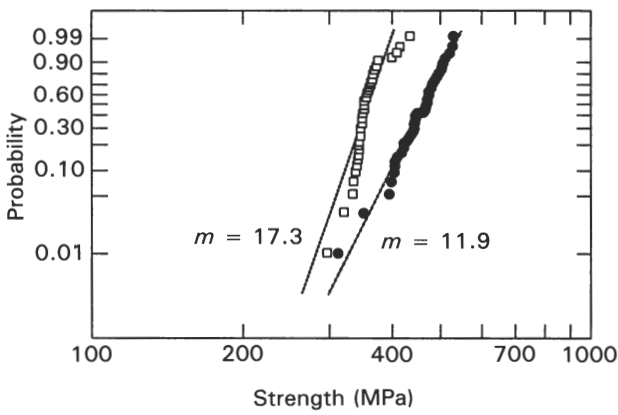


Figure 5 Weibull plots for Ce-TZP ceramics. Coarser material shows higher Weibull modulus. (●) Fine grain, (□) coarse grain.

material with a pronounced *R*-curve. Note that, notwithstanding this flaw tolerance, the strength data still show substantial scatter.

Weibull diagrams for Ce-TZP specimens without indentations are shown in Fig. 5. The Weibull modulus of both Ce-TZP materials is significantly higher than for the Y-TZP, $m = 17.3$ for coarse-grain and $m = 11.9$ for fine-grain material, suggesting a correlation with degree of flaw tolerance.

3.4.3. Mg-PSZ

Indentation–strength data for the Mg-PSZ ceramics are plotted in Fig. 6. The peak-aged material exhibits the highest strengths, followed by the under-aged and the over-aged materials. This is consistent with previous studies [11,14]. The degree of flaw tolerance shows the same trend, i.e. highest for the peak-aged and lowest for the over-aged material.

The Weibull data for the three materials are plotted in Fig. 7. Again, the Weibull modulus correlates with degree of flaw tolerance: $m = 20.0$ for peak-aged, $m = 10.3$ for under-aged, and $m = 6.3$ for over-aged material.

4. Discussion

We have demonstrated flaw tolerance, i.e. failure stress independent of initial flaw size, in zirconia ceramics using the indentation–strength test. This flaw tolerance is especially pronounced in Ce-TZP and Mg-PSZ materials, less so in Y-TZP. In the Ce-TZP and Mg-PSZ, the tolerance increases systematically with increasing degree of t–m transformation during fracture—the same mechanism responsible for the relatively strong *R*-curves in these two zirconias [9, 11, 14, 17, 21]. This increase in transformation activity reflects an increase in Weibull modulus for unindented, polished specimens that fail from processing flaws. There is, therefore, an implied correlation between flaw tolerance, hence *R*-curve, and reliability.

In addressing this potential correlation, we need to consider the nature of the flaws in our zirconia ceramics. We recall from Section 3.3 that indentation cracks tend not to be well developed in these materials, especially in Ce-YZP and Mg-PSZ; they remain

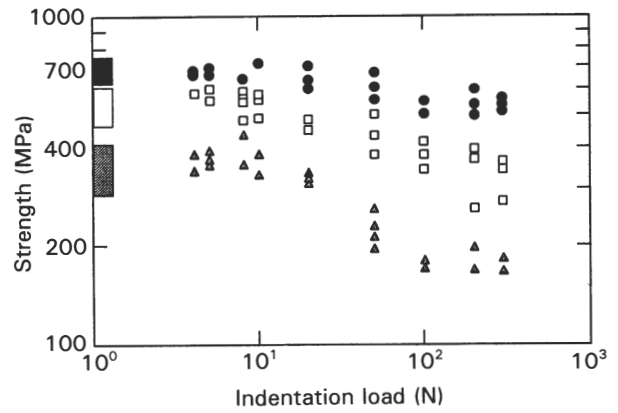


Figure 6 Strength as a function of indentation load for Mg-PSZ ceramics. Materials show enhanced strength and flaw tolerance, in order (●) peak-aged, (□) under-aged and (▲) over-aged.

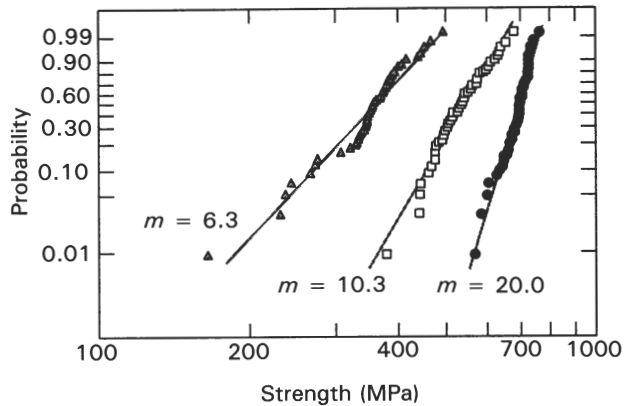


Figure 7 Weibull plots for Mg-PSZ ceramics. Highest Weibull modulus in order (●) peak-aged, (□) under-aged and (▲) over-aged.

constricted at the impression corners within an outer encasing compressive transformation zone [22]. In contrast to other flaw-tolerant ceramics like coarse-grained aluminas where radial cracks are generally well developed [10, 23, 24], the critical conditions for failure are governed more by the mechanics of crack initiation than of crack propagation [23, 24]. The mechanics of initiation within residual contact fields is complex, even in materials with single-valued toughness [24]; the superposition of a transformation surround zone adds to this complexity [22]. Nevertheless, working analytical treatments of this problem are not beyond the bounds of indentation fracture mechanics [22].

The strong similarities in indentation flaw tolerance in such apparently disparate ceramics as our toughened zirconias (notably Figs 4 and 6) and coarsened aluminas [25] are of special interest in light of the above differences in radial crack configuration. Notwithstanding the fact that the radial cracks are comparatively ill-developed in the zirconias, the strength in both material types remains strongly independent of indentation impression size (typically over a range 25–250 μm in diagonal) relative to a classical flaw-size^{-1/2} (load^{-1/3}) response. Moreover, the strengths for low-load indentations in these materials, in contrast to materials without strong toughening (such as

the Y-TZP in Fig. 2), are asymptotic to the strengths for unindented specimens. In this sense indentations may indeed be considered truly representative of natural flaws. These characteristics suggest that all flaws, regardless of history, are *R*-curve stabilized [4, 8, 26, 27], so reducing the sensitivity of strength to initial flaw size. Such flaw insensitivity is not seen in materials with single-valued toughness like glass [24]; there, the scatter in strength in the subthreshold region is typically more than an order of magnitude higher than in the postthreshold radial crack region. In glass there is no *R*-curve mechanism to negate the inherent susceptibility of initiation conditions to small geometrical fluctuations in the size and location of flaw nuclei within the immediate (strongly inhomogeneous) indentation stress fields [24].

The impressive insensitivity of strength to flaw size implicit in Figs 4 and 6 lead us to seek an alternative explanation for the observed strength scatter in our zirconia ceramics, namely in the microstructural variation. Preliminary quantitative analyses of polished surfaces in the SEM reveal a considerable point-to-point variability in grain size in our TZP zirconias. Similar determinations of precipitate size and spacing in the PSZ have yet to be made, but cursory SEM examinations do indicate some tendency for variability in precipitate size. In this context, we may recall from Section 3.4 the strong influence of precipitate size on the strength of Mg-PSZ. The implication is that fluctuations in precipitate size may profoundly influence the shape of the local short-crack *R*-curve, with consequent variation in specimen-to-specimen strengths. Again, it is the distribution in the underlying microstructural characteristics, rather than in the flaw size, that principally determines the variability in these materials. There are profound implications here concerning reliability in material design, with a shift in emphasis from traditional flaw elimination to microstructural characterization and processing control [23].

This shift in emphasis raises stochastic issues. Does the Weibull distribution remain a valid measure of reliability in such cases [7-9, 27]? In the present study we have retained the Weibull diagram simply as a vehicle for data display. Insights into such complex stochastic problems may await the use of computer algorithms to simulate flaw evolution in representative microstructures [28].

Acknowledgements

The authors thank Linda Braun, Nitin Padture, Julie Runyan, Srinivasarao Lathabai and Robert Cook for many helpful discussions, and Terry Deis and Carl

Lovejoy for their help in sample preparation. This research was sponsored by the Air Force Office of Scientific Research.

References

1. R. M. McMEEKING and A. G. EVANS, *J. Am. Ceram. Soc.* **65** (1982) 242.
2. A. G. EVANS and R. M. CANNON, *Acta Metall.* **34** (1986) 761.
3. M. J. READEY, R. W. STEINBRECH and A. H. HEUER, Materials Research Society Symposium Proceedings Vol. 78, edited by P. F. Becher, M. V. Swain and S. Somiya (MRS Press, Pittsburgh, PA, 1987) p. 107.
4. R. F. COOK, B. R. LAWN and C. J. FAIRBANKS, *J. Am. Ceram. Soc.* **68** (1985) 604.
5. D. B. MARSHALL, *ibid.* **69** (1986) 173.
6. S. J. BENNISON and B. R. LAWN, *J. Mater. Sci.* **24** (1989) 3169.
7. K. KENDALL, N. McN. ALFORD, S. R. TAN and J. D. BIRCHALL, *J. Mater. Res.* **1** (1986) 120.
8. R. F. COOK and D. R. CLARKE, *Acta Metall.* **36** (1988) 555.
9. D. K. SHETTY and J. S. WANG, *J. Am. Ceram. Soc.* **72** (1989) 1158.
10. L. M. BRAUN, S. J. BENNISON and B. R. LAWN, *ibid.* **75** (1992) 3049.
11. M. J. READEY, PhD thesis, Case Western Reserve University (1987).
12. D. K. SHETTY, *J. Am. Ceram. Soc.* **76** (1993) 961.
13. R. M. ANDERSON and L. M. BRAUN, *ibid.* **73** (1990) 3059.
14. R. H. HANNINK and M. V. SWAIN, *J. Aust. Ceram. Soc.* **18** (1982) 53.
15. V. GROSS and M. V. SWAIN, *ibid.* **12** (1986) 1.
16. K. TSUKUMA and M. SHIMADA, *Am. Ceram. Soc. Bull.* **65** (1986) 1386.
17. D. J. GREEN, R. H. J. HANNINK and M. V. SWAIN, "Transformation Toughening of Ceramics" (CRC Press, Boca Raton, FL, 1989) p. 90.
18. D. L. PORTER and A. H. HEUER, *J. Am. Ceram. Soc.* **62** (1979) 298.
19. G. QUINN, *ibid.* **73** (1990) 2374.
20. J. D. SULLIVAN and P. H. LAUZON, *J. Mater. Sci. Lett.* **5** (1986) 1245.
21. M. V. SWAIN and L. R. F. ROSE, *J. Am. Ceram. Soc.* **69** (1986) 511.
22. L. M. BRAUN and R. F. COOK, private communication (1993).
23. B. R. LAWN, "Fracture of Brittle Solids", 2nd Edn (Cambridge University Press, Cambridge, 1993) Chs 9, 10.
24. S. LATHABAI, J. RÖDEL, B. R. LAWN and T. P. DABBS, *J. Mater. Sci.* **26** (1991) 2157.
25. P. CHANTIKUL, S. J. BENNISON and B. R. LAWN, *J. Am. Ceram. Soc.* **73** (1990) 2419.
26. Y.-W. MAI and B. R. LAWN, *Ann. Rev. Mater. Sci.* **16** (1986) 415.
27. K. KENDALL, N. McN. ALFORD and J. D. BIRCHALL, Materials Research Society Symposium Proceedings, Vol. 78, edited by P. F. Becher, M. V. Swain and S. Somiya (MRS Press, Pittsburgh, PA, 1987) p. 189.
28. W. CURTIN, private communication (1992).

Received 26 February
and accepted 27 April 1993